Acoustic simulation of an induction machine with squirrel-cage rotor

C. Schlensok, D. van Riesen, T. Küest and G. Henneberger
Institute of Electrical Machines, RWTH Aachen University, Aachen, Germany

Abstract

Purpose – To present results of research closely linked to real life applications and to resume the work of a period of a few years.

Design/methodology/approach – The combination of finite-element method (FEM) and boundary-element method is applied to simulate the electromagnetic, mechanical, and acoustic behaviour of an induction machine with squirrel-cage rotor. The paper gives an overall view of the workflow and the implemented mathematics, starting off with the two-dimensional, transient electromagnetic simulation and the succeeding three-dimensional, static electromagnetic simulation. Theory and results of the mechanical and acoustic simulations are discussed.

Findings – A main result of the research work is that the simulation of the acoustic behaviour of an electrical machine is very time-consuming. Furthermore, geometry adoption, especially of the mechanical model, is very sensible.

Research limitations/implications – Using the FEM for simulation of structure dynamic problems is often limited to how the boundary layers are handled. In real life materials are not "connected" but glued or clamped. Therefore, the behaviour can only be adapted by manipulating the material parameters. There are other methods known for simulation, which could be applied. On the other hand, measurements could be used for iterative parameter adoption.

Practical implications – A significant result of the work is that the results obtained only allow for comparison. Exactness is more a question of modelling the real behaviour than matching the results to measurement in terms of values.

Originality/value – This paper gives an overview of how to simulate the complete chain from electromagnetics to acoustics of an electric machine.

Keywords Acoustics, Simulation, Induction, Finite element analysis

Paper type Research paper

1. Introduction

Owing to the customer's satisfaction the acoustics in cars are getting more and more part of research. Nowadays, there are many electromagnetic devices in cars, which have replaced mechanical systems. One example for this trend is an electrical machine replacing the hydraulic power-steering drive. In this paper, an induction machine with squirrel-cage rotor is analysed regarding the electromagnetically excited audible noise. This motor is employed as power-steering drive. The aim of this work is to predict the noise generated by the device. The machine is simulated using the finite-element method (FEM) for the electromagnetic and a structure-dynamic model and the boundary-element method (BEM), for the noise estimation.

COMPEL: The International Journal for Computation and Mathematics in Electrical and Electronic Engineering
Vol. 25 No. 2, 2006
pp. 475-486

0332-1649
DOI 10.1108/03321640610649131

2. FEM/BEM simulation

The computational process of acoustic simulation of the induction machine is divided into three steps:

(1) electromagnetic FEM simulation;

(2) structure-dynamic FEM computation; and the

(3) acoustic BEM calculation.

For all three steps models of the machine geometry have to be built and discretized which take the relevant parts of the machine into account, respectively.

2.1 Electromagnetic simulation

In the case of induction machines with squirrel-cage rotor the rotor-bar currents are unknown. Therefore, a transient simulation, which takes the rotational movement into account, has to be performed. In order to reduce the computation time and cost the machine is calculated in two dimensions at first. The $\vec{A}$-formulation used in the solver iMOOSE.tsa2d reads:

$$\int_\Gamma \left(\nabla \alpha_i v \nabla A_z(t) + \alpha_i \sigma \frac{\partial}{\partial t} A_z(t) \right) \mathrm{d}\Gamma = \int_\Gamma \left(\alpha_i J_{z0}(t) + \nabla \times (\alpha_i \vec{e}_z) \cdot v \vec{B}_r \right) \mathrm{d}\Gamma, \quad \forall i = 1, 2, \ldots, n_n. \tag{1}$$

The equation given in Galerkin formulation (Bastos, 2003) is solved in the entire model region Γ. The material parameters v and σ represent the non-linear reluctivity and the linear conductivity. The shape function of an element is defined by α_i. First-order triangular shaped elements are used. $J_{z0}(t)$ describes the z-component of the given coil current-density and $\vec{B}_r$ is the remanence of possible permanent magnets which of course do not exist in induction machines. For linear interpolation of the time-dependent variables the first-order time-step algorithm is applied and $A(t)$ can be written as a function of time:

$$A(t) = (1 - \Theta) A_n + \Theta A_{n+1} \tag{2}$$

$$\Theta = \frac{t - t_n}{t_{n+1} - t_n} = \frac{t - t_n}{\Delta t}; \quad 0 \leq \Theta \leq 1 \tag{3}$$

$\Theta$is the weighting parameter and set to $\Theta = 2/3$ according to the Galerkin scheme (Zienkiewicz and Taylor, 1989). Setting $\Theta = 2/3$ results in fastest convergence for the transient simulation.

The induction machine regarded has $N_S = 36$ stator and $N_R = 26$ rotor slots. Owing to the number of rotor slots the motor shows a 180° symmetry. Therefore, a half (180°) FEM-model is used. The 2D electromagnetic model consists of 6,882 first-order, triangular elements. 4,000 time steps are calculated at rated speed $n_N = 1{,}200$ rpm and a stator frequency of $f_1 = 48.96$ Hz. The resulting torque behaviour of the transient simulation is shown in Figure 1. When the transient phenomenon has died out the time behaviour is analysed. The average torque is $T_{2D} = 4.312$ Nm.

With:

$$J_z = -\sigma \frac{A_{z_{n+1}} - A_{z_n}}{\Delta t} \tag{4}$$

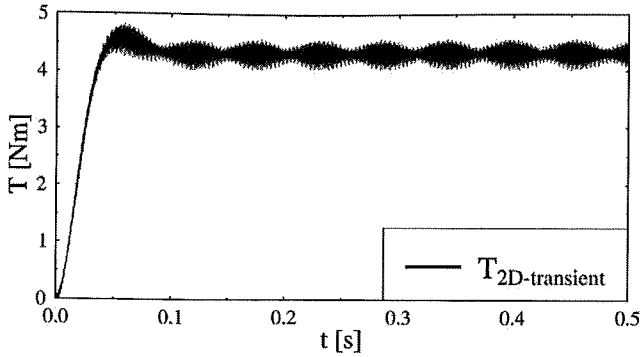

Figure 1.
Resulting torque obtained from the 2D model

the rotor-bar current-density J_z is evaluated. A_z is the z-component of the magnetic vector potential $\vec{A}$. The conductivity of the rotor bars is represented by σ. The time step is Δt.

Figure 2 shows the resulting rotor-bar currents for four bars. The frequency is the slip frequency $f_2 = 8.96$ Hz. The maximal current amplitude reached for all bars is $I_{\max} = 248.32$ A and the amplitude of the fundamental is $\hat{I}_1 = 220.86$ A. The first significant harmonic order is the fifth-order of the stator frequency at $f_5 = 244.8$ Hz with $\hat{I}_5 = 23.15$ A which is modulated with twice the slip frequency: $f = 226.88$ and 262.72 Hz.

The resulting current densities are used by the static, three-dimensional FEM model, which computes the machine using iMOOSE.stat3d. The 3D static electromagnetic solver formulation applying the magnetic vector potential $\vec{A}$ in Galerkin scheme reads (Kost, 1994):

$$\int_\Omega \nabla \times \vec{\alpha}_i v \nabla \times \vec{A}\, \mathrm{d}\Omega = \int_\Omega (\vec{\alpha}_i \cdot \vec{J}_0 + \nabla \times \vec{\alpha}_i \cdot v\vec{B}_r)\, \mathrm{d}\Omega, \quad \forall i = 1, 2, \ldots, n_n. \tag{5}$$

Both solvers from equations (1) and (5) are part of the open-source software iMOOSE (Arians *et al.*, 2006).

The FEM-model consists of 288,782 first-order tetrahedral elements. For computation-time saving-reasons the axial length of the model is reduced to a third of the iron length. The skewing angle (front to back angle) is kept the same. Figure 3 shows the electromagnetic model of the motor.

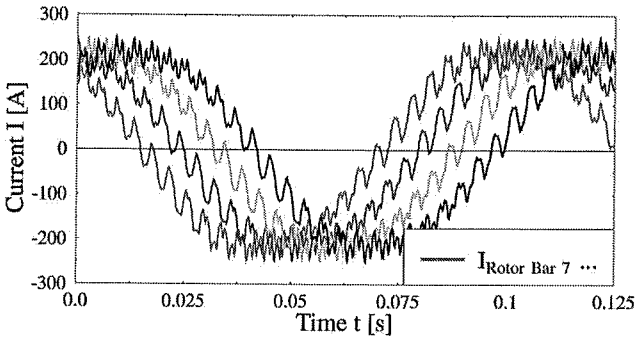

Figure 2.
Resulting rotor-bar currents for four rotor bars obtained from the 2D model

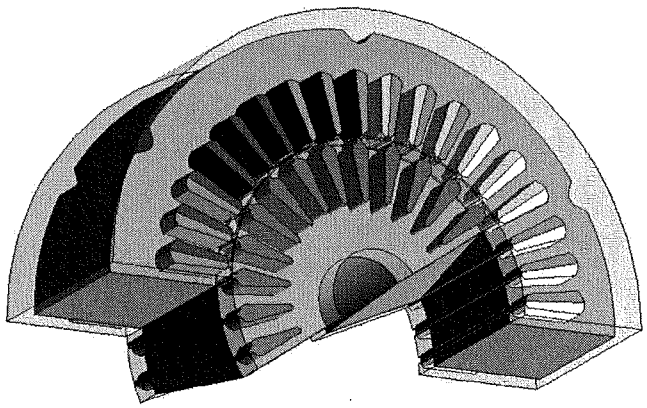

Figure 3.
3D FEM model for electromagnetic simulation

The stator winding head and the short-circuit ring of the rotor are reduced to extended bars, which are surrounded by air. This allows a more realistic consideration of the front leakage than in case of the 2D model. There, of course, no front leakage can be regarded. The figure also shows the two-layer winding of the stator and the complicated modelling of the skewed rotor. To avoid the slicing of rotor bars which would result in current excitations very difficultly to compute the rotor is modelled in such a way that it is twisted in the same way the bars are.

The machine is calculated at $N = 120$ rotor positions. The skewing of the rotor is kept the same. The mechanical angle between each static time step is $\Delta\alpha = 3°$.

The machine's skewing angle is $\gamma = 10°$. For each time step the rotor is detached from the stator, rotated, and reattached. The models are generated automatically with the FEM-tool (ANSYS Inc., www.ansys.com). Figure 4 exemplary shows the flux-density distribution for one time step.

2.2 Structure-dynamic simulation

From the flux-density distribution the surface-force density on the stator teeth can be derived using the Maxwell-stress tensor (Kost, 1994; Ramesohl *et al.*, 1996). The formulation reads:

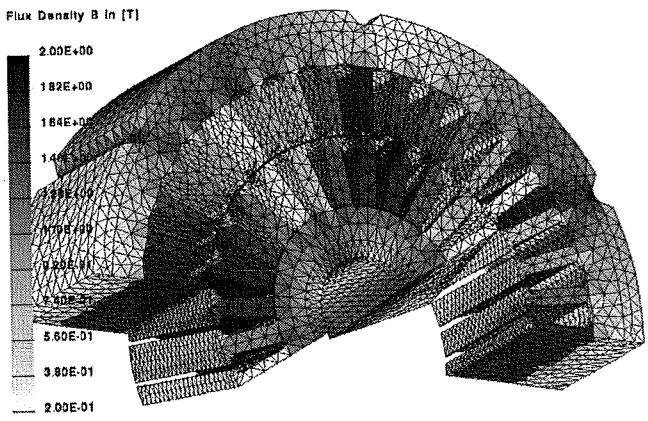

Figure 4.
Flux-density distribution for the 3D model

$$\vec{\sigma} = \frac{1}{2}\vec{n}_{12}\left[B_n(H_{1n} - H_{2n}) - (w'_1 - w'_2)\right]. \quad (6)$$

The index n represents the normal components of $\vec{B}$ and $\vec{H}$. $\vec{n}_{12}$ is the normal vector of the boundary surface from region 2 to 1. w'_1 and w'_2 are the magnetic co-energy densities of these regions. Lorentz forces and forces stemming from magnetostriction can be neglected since they are much lower than the electromagnetic forces.

Figure 5 shows the surface-force density distribution for one time step. See also Figure 6.

The skewing of the rotor is reflected in the force excitation of the stator teeth. Depending on the rotational direction the up-running edge of each tooth is excited highest on the front or on the back side.

In a next step the force excitation is analysed. For each element of the stator teeth connected to the air gap the values of all time steps are collected and then transformed into the frequency domain using the fast-Fourier transformation (FFT) (Bronstein and Semendjajew, 1991). This is a very time intensive step in the acoustic analysis of an electrical machine, because the data is distributed to each time step but must be assigned to each element. This means, that for each of the 20,602 stator-teeth surface elements, which are connected to the air gap, 120 force-density values must be collected and analysed using the FFT. Finally the FFT values must be resorted to two files per frequency, which hold the imaginary and the real part of the surface-force density excitation. The resulting spectrum (absolute values) for one single stator-tooth element is shown in Figure 7.

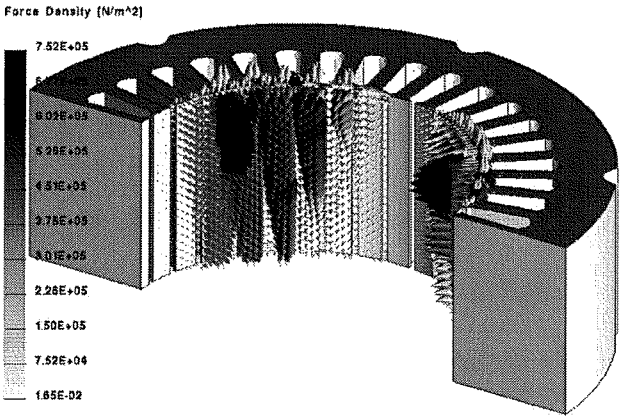

Figure 5.
Surface-force density distribution on the stator teeth for one time step (only stator lamination shown)

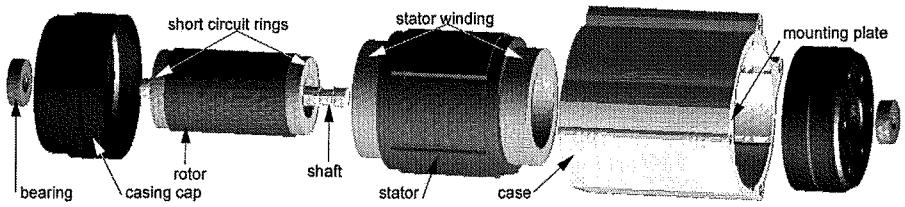

Figure 6.
Exploded view of the structure-dynamic model of the induction machine with squirrel-cage rotor

Owing to the time step Δt and the number of time steps N the cut-off frequency is $f_{co} = 1{,}200$ Hz with $\Delta f = 20$ Hz which is equal to the rotor speed. The harmonic orders detected in the spectrum are the double stator frequency (97.92 Hz), the first and second rotor slot harmonic (520 and 1,040 Hz), and their modulations with the double stator frequency (Schlensok *et al.*, 2003; Nau, 2000; Jordan, 1950). The harmonic orders with the highest magnitudes are selected for the further study.

The next step is to calculate the deformation of the entire structure of the machine. Therefore, a complete mechanical model of the machine must be generated consisting of the stator and rotor with their windings, the shaft, the case, the bearings, and the casing caps. In order to reduce the number of finite elements the rotor is simplified and modelled as a cylinder. The stator tooth geometry is reduced to a rectangular shape. The number of first-order tetrahedral elements of the mechanical model is 90,065. The solver transforms the first-order elements to second-order. Figure 6 shows an exploded view of the entire model.

With the mechanical model the deformation of the structure of the induction machine is computed for the selected frequencies in the following step. Therefore, the surface-force density excitation is transformed from the electromagnetic model to the mechanical model for each of the selected frequencies.

The deformation-solver formulation reads (Ramesohl, 1999):

$$\mathbf{K}\cdot\mathbf{D} + \mathbf{F}\cdot\dot{\mathbf{D}} + \mathbf{M}\cdot\ddot{\mathbf{D}} = \mathbf{R} \tag{7}$$

K is the matrix of the stiffness of all elements of the model, **M** represents the mass, **F** is the damping, **D** is the deformation, and **R** is the exciting force. Owing to harmonic analysis equation (7) is simplified to:

$$(\mathbf{K} - \omega^2\mathbf{M} + \mathrm{j}\omega\mathbf{F})\cdot\mathbf{D} = \mathbf{R}. \tag{8}$$

$\omega = 2\pi f$ is the angular frequency. The damping **F** can be neglected since the mechanical model consists of material with high elastic stress modules. If for instance rubber is used the damping cannot be neglected. Therefore, the solver is not able to regard such elastic materials. Initial tension is not regarded as well. Usually, initial tension mainly arises from temperature effects which are not subject of the investigations.

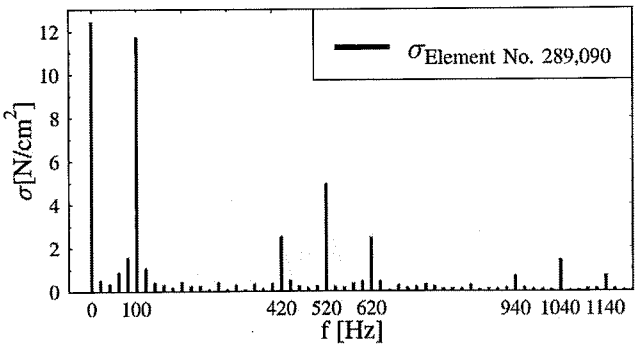

Figure 7.
Spectrum of the surface-force density excitation of one single stator-tooth surface element (absolute-values)

K is the sum of all element-stiffness matrices $\mathbf{k}_i$:

$$\mathbf{K} = \sum_{i=1}^{n} \mathbf{k}_i = \sum_{i=1}^{n} \int_{\Omega_i} \mathbf{B}_i^{\mathrm{T}} \cdot \mathbf{H}_i \cdot \mathbf{B}_i \, \mathrm{d}\Omega_i. \tag{9}$$

$\mathbf{H}_i$ is the elasticity matrix for each element (Zienkiewicz and Taylor, 1989):

$$\mathbf{H}_i = \frac{E(1-v)}{(1+v)(1-2v)} \begin{pmatrix} 1 & a & a & 0 & 0 & 0 \\ a & 1 & a & 0 & 0 & 0 \\ a & a & 1 & 0 & 0 & 0 \\ 0 & 0 & 0 & b & 0 & 0 \\ 0 & 0 & 0 & 0 & b & 0 \\ 0 & 0 & 0 & 0 & 0 & b \end{pmatrix}. \tag{10}$$

with:

$$a = \frac{v}{1-v} \quad \text{and} \quad \mathrm{b} = \frac{1-2v}{2(1-v)}. \tag{11}$$

ν is Poisson's ratio and E the elastic modulus. $\mathbf{B}_i$ is the differential matrix for the elements, where $\mathbf{B}_i^{\mathrm{T}}$ is the transposed of it. With $\alpha_1 \ldots \alpha_4$ being the degrees of freedom of the first-order tetrahedral elements $\mathbf{B}_i$ reads (Ramesohl, 1999):

$$\mathbf{B}_i = \begin{pmatrix} \frac{\partial \alpha_1}{\partial x} & 0 & 0 & \ldots & \frac{\partial \alpha_4}{\partial x} & 0 & 0 \\ 0 & \frac{\partial \alpha_1}{\partial y} & 0 & \ldots & 0 & \frac{\partial \alpha_4}{\partial y} & 0 \\ 0 & 0 & \frac{\partial \alpha_1}{\partial z} & \ldots & 0 & 0 & \frac{\partial \alpha_4}{\partial z} \\ \frac{\partial \alpha_1}{\partial y} & \frac{\partial \alpha_1}{\partial x} & 0 & \ldots & \frac{\partial \alpha_4}{\partial y} & \frac{\partial \alpha_4}{\partial x} & 0 \\ 0 & \frac{\partial \alpha_1}{\partial z} & \frac{\partial \alpha_1}{\partial y} & \ldots & 0 & \frac{\partial \alpha_4}{\partial z} & \frac{\partial \alpha_4}{\partial y} \\ \frac{\partial \alpha_1}{\partial z} & 0 & \frac{\partial \alpha_1}{\partial x} & \ldots & \frac{\partial \alpha_4}{\partial z} & 0 & \frac{\partial \alpha_4}{\partial x} \end{pmatrix} \tag{12}$$

The matrices **M**, **F**, **D**, and **R** of equations (7) and (8) are built in an analogue way to **K** from equation (9). In order to solve the boundary-value problem of the deformations entirely a boundary condition must be regarded. It is necessary to define at least one node of the model, which is fixed. This is a Dirichlet condition. Here, the surface nodes of the mounting plate are selected and fixed in the solving process (Figure 6).

Figure 8 shows exemplarily the strongly emphasized real part of the deformation of the stator lamination and the casing for $f = 620$ Hz. The emphasizing factor is set to 6,750,000.

Owing to the even number of pole pairs $p = 2$ and the even number of rotor slots $N_{\mathrm{R}} = 26$ of the induction machine the mechanical orders of deformation can only be even numbers as well: $r = 0, 2, 4, \ldots$ (Seinsch, 1992). Some orders found are shown in Figure 9. $r = 2$ is found for $f = 720$ Hz, $r = 4$ for $f = 1{,}040$ Hz, and $r = 6$ for

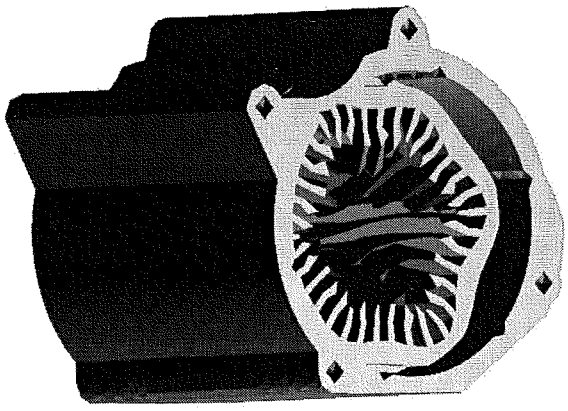

(a) Deformation of Stator and Casing

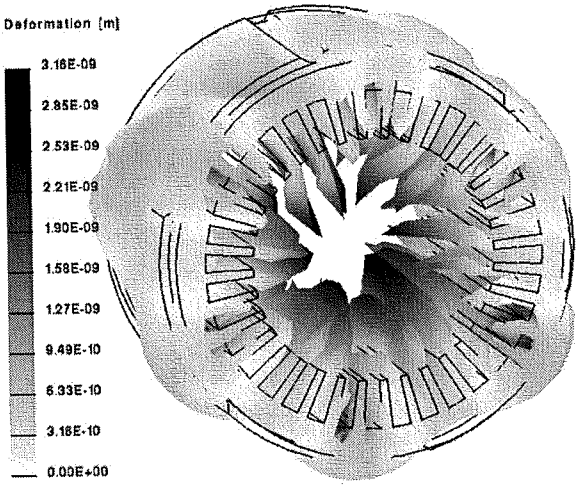

(b) Deformation of Stator

Figure 8.
Real part of the deformation for $f = 620$ Hz

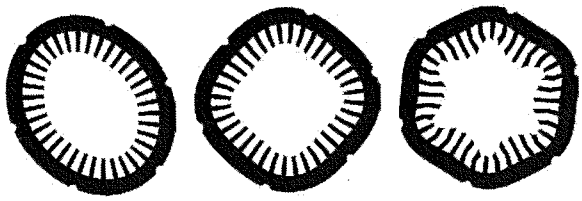

(a) $r = 2$ (b) $r = 4$ (c) $r = 6$

Figure 9.
Mechanical orders of deformation

$f = 620$ Hz. Small mechanical orders have the strongest impact in respect of the deformation amplitude. For this reason, numbers greater than $r = 6$ can be neglected in general (Figure 9).

The deformation of the structure of the machine can be used for the acoustic simulation described in the following section. Alternatively, the body sound can be derived from its results. Here, simulation results are compared to acceleration measurements performed by the industrial partner. The reference value is $a_{ref} = 1\,m/s^2$ and the level L_S is defined by:

$$L_S = 20 \log \frac{a}{a_{ref}} \, dB. \tag{13}$$

a is the acceleration of the specific node at the regarded frequency f, which is derived from the displacement u. $\omega = 2\pi f$ is the angular frequency. In respect of the sinusoidal deformation the acceleration vector is defined by:

$$\vec{a} = \begin{pmatrix} a_{tan} \\ a_{rad} \\ a_{axial} \end{pmatrix} = \begin{pmatrix} -\omega^2 u_{tan} \\ -\omega^2 u_{rad} \\ -\omega^2 u_{axial} \end{pmatrix} \tag{14}$$

with:

$$\frac{\partial^2 u(t)}{\partial t^2} = \frac{\partial^2}{\partial t^2} \hat{u} \cos(j\omega t - \varphi) = -\omega^2 u(t). \tag{15}$$

φ is the phase angle and $j^2 = -1$. The displacement is a vector of complex numbers in Cartesian coordinates:

$$\vec{\underline{u}} = \begin{pmatrix} \underline{x} \\ \underline{y} \\ \underline{z} \end{pmatrix} = \begin{pmatrix} \Re\{\underline{x}\} + j\Im\{\underline{x}\} \\ \Re\{\underline{y}\} + j\Im\{\underline{y}\} \\ \Re\{\underline{z}\} + j\Im\{\underline{z}\} \end{pmatrix}. \tag{16}$$

In order to provide the displacement vector as local coordinates with tangential, radial, and axial component the following transformation has to be performed:

$$\vec{\underline{u}}_{local} = \begin{pmatrix} \underline{u}_{tan} \\ \underline{u}_{rad} \\ \underline{u}_{axial} \end{pmatrix} = \begin{pmatrix} \vec{\underline{u}} \cdot \vec{e}_{tan} \\ \vec{\underline{u}} \cdot \vec{e}_{rad} \\ \vec{\underline{u}} \cdot \vec{e}_{axial} \end{pmatrix} = \begin{pmatrix} \underline{x} \cdot \vec{e}_x \cdot \vec{e}_{tan} + \underline{y} \cdot \vec{e}_y \cdot \vec{e}_{tan} + \underline{z} \cdot \vec{e}_z \cdot \vec{e}_{tan} \\ \underline{x} \cdot \vec{e}_x \cdot \vec{e}_{rad} + \underline{y} \cdot \vec{e}_y \cdot \vec{e}_{rad} + \underline{z} \cdot \vec{e}_z \cdot \vec{e}_{rad} \\ \underline{x} \cdot \vec{e}_x \cdot \vec{e}_{axial} + \underline{y} \cdot \vec{e}_y \cdot \vec{e}_{axial} + \underline{z} \cdot \vec{e}_z \cdot \vec{e}_{axial} \end{pmatrix}. \tag{17}$$

The three components of the local coordinate systems are equal to those of a global cylindrical coordinate system with the axial component in direction of the shaft, the radial is normal onto the rotor cylinder and the tangential in direction of the angle φ (Bronstein and Semendjajew, 1991).

Table I shows some results of the body sound-simulation. The highest amplitudes are reached for the first rotor-slot harmonic at $f_{26} = 26 f_R = 520$ Hz, the first stator-slot harmonic $f_{36} = 36\ f_R = 720$ Hz, $f = 940$ and 1,040 Hz. The level for the axial component shows the smallest values in all cases. These results suit the acceleration measurements performed by the industrial partner in a reasonable way.

2.3 Acoustic simulation

The last step of the analysis is the acoustic simulation of the machine. Acoustic noise is a result of the deformation of the surface of a body. Therefore, only the deformation of the surfaces has to be taken into account and the BEM is applied for the acoustic simulation. The equation to be solved reads:

$$\mathbf{H}\underline{p} = \mathbf{G} \cdot \underline{\vec{v}}. \tag{18}$$

$\underline{p}$ is the complex sound pressure which is the result of the acoustic simulation and $\underline{\vec{v}}$ is the complex velocity vector of all nodes of the BEM model.

For the acoustic simulation a third model of the machine is generated by extracting the surface mesh of the structure-dynamic model. The resulting model consists of 7,998 triangular shell elements (Figure 10).

After the acoustic model has been simulated the sound pressure is estimated in a post-processing step. An analysis hemisphere is located in a distance of $d = 1\,\mathrm{m}$ around the machine. The induction machine is positioned in the centre of the ground plane. The ground plane itself is reverberant. Of course, different analysis surfaces like spheres and planes are possible. On the surface of the hemisphere the sound pressure p

f (Hz)	$L_{S,\,rad}$ (dB)	$L_{S,\,tan}$ (dB)	$L_{S,\,axial}$ (dB)
100	59.4	58.5	44.0
420	85.2	83.8	68.4
520	82.6	82.1	66.9
620	59.9	64.5	48.5
720	85.4	84.2	68.8
940	88.5	87.5	46.8
1,040	82.4	80.5	55.7
1,140	67.7	67.0	51.4

Table I.
Results of the body sound-simulation

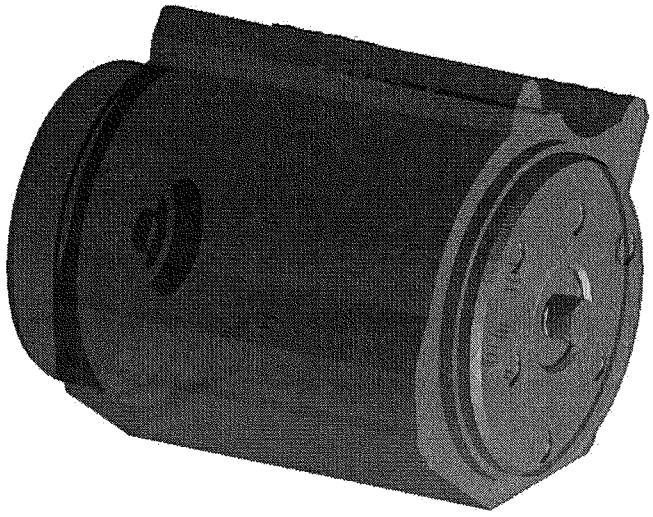

Figure 10.
The acoustic BEM-model of the machine

from equation (18) is computed. The values of the sound pressure spread over a wide range. For this reason, the sound-pressure values are transformed to a level:

$$L_p = 20 \log\left(\frac{p}{p_0}\right) \mathrm{d}B. \tag{19}$$

$p_0 = 2 \times 10^{-5}$ N/m^2 is the auditory threshold at 1,000 Hz.

Figure 11 shows exemplarily the sound-pressure distribution for $f = 520$ Hz. There are some extinction effects on the topside of the hemisphere. Here, the maximum sound level reached is about $L_{p,\max} = 23$ dB.

Table II collects the computed maximum sound-pressure levels for some selected frequencies. Although the highest force excitation is found for $f = 100$ Hz (Figure 7) the resulting sound pressure on the hemisphere is the lowest. Its value is even below the auditory threshold. The highest levels are reached for the first stator- and rotor-slot harmonics at $f = 520$ and 720 Hz as well as at $f = 940$ Hz. These relations suit the structure-borne sound-measurements mentioned in the previous section by the proportion of the orders.

3. Conclusion

In this paper, the simulation of the electromagnetically excited structure- and air-borne noise of an induction machine with squirrel-cage rotor is described. The acoustic simulation is performed in three main steps and requires two FEM- and one BEM-model of the geometry of the machine. The structure-borne sound is derived from an intermediate step. The theory of the electromagnetic solvers is described as well as that of the structure-dynamic and the acoustic.

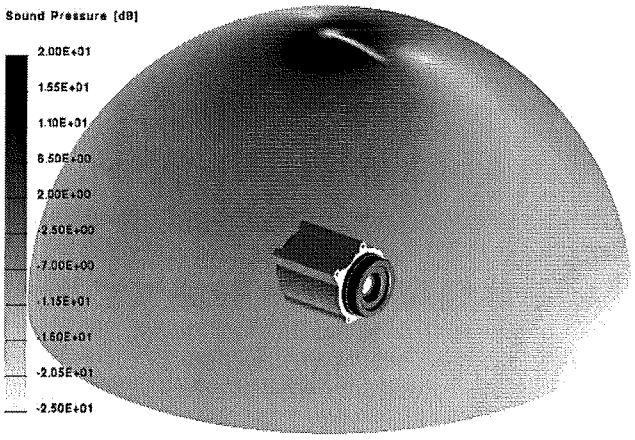

Figure 11.
Sound-pressure distribution for $f = 520$ Hz

f (Hz)	$L_{p,\max}$ (dB)	f (Hz)	$L_{p,\max}$ (dB)
100	−16	420	16
520	23	620	9
720	27	940	28
1,040	11	1,140	9

Table II.
Values for $L_{p,\max}$ for selected frequencies

The main aspects which have to be regarded during the simulation are pointed out and some example pictures and tables show qualitative results. Detailed results have been presented in an additional paper concerning different types of surface-force excitation in the induction machine (Schlensok and Henneberger, 2004).

It is now possible to estimate the acoustic behaviour of electrical devices. The structure-borne sound allows for simulating the deformation of the structure which is transmitted to other parts of the structure, e.g. the interior of a car.

References

Arians, G., Bauer, T., Kaehler, C., Mai, W., Monzel, C., Schlensok, C. and van Riesen, D. (2006), "iMOOSE", available at: www.imoose.de

Bastos, J.P.A. (2003), *Electromagnetic Modeling by Finite Element Methods*, Marcel Dekker, Inc., New York, NY.

Bronstein, I.N. and Semendjajew, K.A. (1991), *Taschenbuch der Mathematik*, B.G. Teubner Verlagsgesellschaft, Stuttgart.

Jordan, H. (1950), *Geräuscharme Elektromotoren*, Verlag W. Girardet, Essen.

Kost, A. (1994), *Numerische Methoden in der Berechnung Elek-tromagnetischer Felder*, Springer, Berlin.

Nau, S.L. (2000), "Acoustic noise of induction electric motor: causes and solutions", paper presented at the 2nd International Seminar on Vibrations and Acoustic Noise in Electric Machinery, September, Lodz.

Ramesohl, I.H. (1999), *Numerische Geräuschberechnung von Drehstom-Klauenpolgeneratoren*, Shaker-Verlag, Aachen.

Ramesohl, I.H., Küppers, S., Hadrys, W. and Henneberger, G. (1996), "Three dimensional calculation of magnetic forces and displacements of a claw-pole generator", *IEEE Trans.-Mag.*, Vol. 32/3, pp. 1685-8.

Schlensok, C. and Henneberger, G. (2004), "Comparison of stator and rotor force excitation for the acoustic simulation of an induction machine with squirrel cage rotor", paper presented at the 16th International Conference Electrical Machines (ICEM 2004), September, Krakow.

Schlensok, C., Schneeloch, G. and Henneberger, G. (2003), "Analysis of stator-teeth forces in induction machines with squirrel cages using 2D-FEM", paper presented at the 6th International Symposium on Electric and Magnetic Fields (EMF 2003), October, Aachen.

Seinsch, H.O. (1992), *Oberfelderscheinungen in Drehfeldmaschinen*, B.G. Teubner, Stuttgart.

Zienkiewicz, O.C. and Taylor, R.L. (1989), *The Finite Element Method*, McGraw-Hill, London.

Corresponding author
C. Schlensok can be contacted at: Christoph.Schlensok@iem.rwth-aachen.de